IOPscience iopscience.iop.org

Home Search Collections Journals About Contact us My IOPscience

Electronic structure and localization behaviour in the GaAs/AlAs Fibonacci superlattice

This article has been downloaded from IOPscience. Please scroll down to see the full text article.

1992 J. Phys.: Condens. Matter 4 5947

(http://iopscience.iop.org/0953-8984/4/27/012)

View the table of contents for this issue, or go to the journal homepage for more

Download details:
IP Address: 171.66.16.159
The article was downloaded on 12/05/2010 at 12:17

Please note that terms and conditions apply.

J. Phys.: Condens. Matter 4 (1992) 5947–5958. Printed in the UK

Electronic structure and localization behaviour in the GaAs/AlAs Fibonacci superlattice

Kenji Hirose†, David Y K Ko‡ and Hiroshi Kamimura§

† Department of Physics, University of Tokyo, 7-3-1 Hongo, Bunkyo-ku, Tokyo, Japan 113

‡ Department of Theoretical Physics, University of Oxford, Oxford OX1 3NP, UK

§ Department of Applied Physics, Science University of Tokyo, 1-3 Kagurazaka, Shinjuku-ku, Tokyo, Japan 162

Received 24 February 1992

Abstract. We study the electronic structure of the GaAs/AlAs Fibonacci superlattice using a semi-empirical sp^3s^* tight-binding method. We find that a self-similar energy spectrum can be seen in the band structure, although the energy spectrum depends strongly on the wavevector parallel to the layers. Furthermore, we find that a localization character is enhanced due to the band hybridization, producing a spiky density of states and a localization-like effect of the wavefunctions in the hybridized energy region. The reasons for the localization-like behaviour are discussed briefly.

1. Introduction

In recent years much attention has been focused on the studies of quasiperiodic systems. This is due to the critical properties these systems have in their electronic structures, and due to the surprising discovery in 1984 of Al–Mn alloys with an icosahedral symmetry diffraction pattern [1, 2]. Among a number of quasiperiodic models, the Fibonacci system, which is the one-dimensional version of quasicrystals, has been of much interest as a model of the quasicrystals. This system has been extensively investigated in the single-band tight-binding limit. Two special cases are usually considered. The first, known as the on-site model, has all the hopping transfer interaction $t_{ij} = t$ constant and the on-site energies V_n take two values arranged in a Fibonacci sequence. The second, the transfer model, has the on-site energies $V_i = V$ constant but the hopping transfer interactions t_{ij} taking on two values, arranged in a Fibonacci sequence. In both cases it is known that the energy spectrum is self-similar, that is, the energy band divides into three subbands, each of which further divides into three, and so on [3–7], creating a singular continuous energy spectrum which reduces in the infinite limit to a Cantor-set spectrum with dense energy gaps everywhere [8–11]. Another property of the Fibonacci quasicrystal is that the wavefunctions are all critical irrespective of their energies, in the sense that they are neither extended nor localized. It should be noted, however, that their decay in the single-band limit is still slow such that they extend over many sites.

Experimentally, Merlin and coworkers [12, 13] were the first to succeed in growing a semiconducting Fibonacci superlattice using GaAs and AlAs. X-ray and Raman

0953-8984/92/275947+12$04.50 © 1992 IOP Publishing Ltd

scattering measurements have confirmed the quasiperiodic crystal and phonon structure. More recently, Yamaguchi *et al* [14] observed a self-similar structure in the energy spectrum of the Fibonacci superlattice using time-resolved 'wide-well' photoluminescence. They have also found that the electron transport properties are intermediate between those of periodic and random superlattices. Most theoretical analysis to date has been concentrated on simple single-band models in 1D, and the effects of the full crystalline structure of GaAs/AlAs on the quasiperiodicity have remained unexplored. In the present paper we investigate the electronic structures and localization behaviour of the GaAs/AlAs Fibonacci superlattice using a semi-empirical sp^3s^* tight-binding method. This allows us to include simply the effect of the band hybridization as well as full three-dimensionality.

In the next section the method and the crystal structure of the GaAs/AlAs Fibonacci superlattice will be described. The results on the energy spectrum and the behaviour of the wavefunctions are presented in section 3. The interplay between the band hybridization and the long-range quasiperiodicity is further investigated numerically by a two-band tight-binding model in section 4. Finally we summarize the results in section 5.

2. Method

The GaAs/AlAs Fibonacci superlattice is constructed by arranging atomic layers of GaAs and AlAs in a Fibonacci sequence. Since the Fibonacci system is not periodic we use a rational approximation and consider a finite F_n layers, where F_n is a Fibonacci number defined by $F_n = F_{n-1} + F_{n-2}$ with $F_1 = 1$, $F_2 = 2$, n is the generation constant, and we apply periodic boundary condition. In order that a long-range quasiperiodicity may be included, we restrict the units of construction of our system to single monolayers of GaAs and AlAs only. Using periodic boundary condition, we have calculated the electronic structures up to the 12th generation which consists of a total of 144 GaAs layers and 89 AlAs layers. In figure 1 we show the schematic crystal structure of the present Fibonacci superlattice.

The calculation is performed with a semi-empirical tight-binding method. sp^3s^* orbitals [15, 16] are used. The atomic state is expressed in the LCAO approximation as

$$\Psi_k^l(r) = \frac{1}{\sqrt{N}} \sum_j^{2F_n} \sum_\alpha^5 C_{j,k}^{\alpha,l} \exp(ik \cdot R_j) \phi_\alpha(r - R_j) \tag{1}$$

where α denotes orbital states s, p_x, p_y, p_z, s^* and j, l, N denote the site number, the band index and the number of atoms in a unit cell respectively. The parameters are chosen to reproduce the experimentally determined band structures of bulk GaAs and AlAs. Second-nearest neighbour interactions are also introduced so as to reproduce the L-point energies. Details of this calculation are given in references [17, 18]. The valence band offset at the Γ point is taken to be 0.50 eV. Spin–orbit interaction has not been included. By diagonalizing the Hamiltonian, we obtain the energy spectrum and the amplitudes of the wavefunctions.

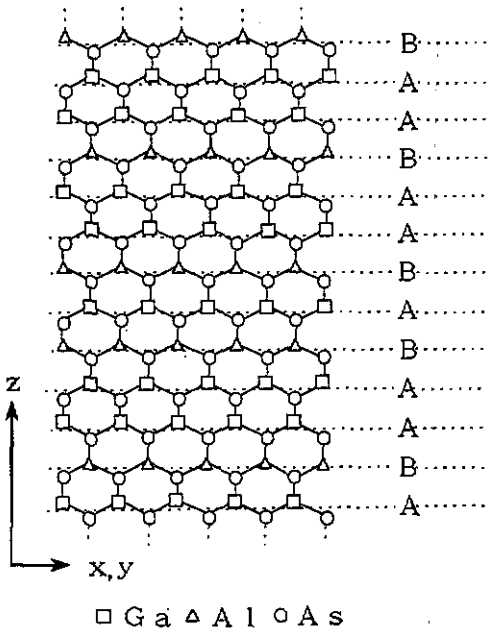

Figure 1. Schematic crystal structure of the present Fibonacci superlattice which consists of monolayer GaAs and monolayer AlAs.

3. Calculated results

Figure 2 shows the calculated band structure of a 12th generation Fibonacci superlattice. The dispersion is shown in a plane perpendicular to the superlattice direction. As a reference, the positions of the energy levels in the bulk GaAs and AlAs are indicated by arrows on the right-hand side of the figure.

First we examine the valence band, which shows two distinct types of dispersion. The set which reaches the X point in the diagram has a smaller dispersion and originates from the heavy hole bands, and the set which extend downwards beyond the bottom of the diagram originates from the light hole bands. In this calculation, the heavy hole band remains doubly degenerate owing to the lack of spin–orbit interaction. We can see that the heavy hole band is divided into three subbands around the Γ point, as expected for a simple Fibonacci system. The light hole band, in contrast, is much wider and no characteristic Fibonacci structure is seen. At the X point, however, the Fibonacci structure collapses into a number of highly degenerate states. This degeneracy comes from a flat energy dispersion along the superlattice direction and suggests that the superlattice X point is special.

As for the conduction band, the states at the X point again are degenerate at a number of energy levels, with no Fibonacci structure observable. At the bottom of the conduction band near the Γ point, we can see that the parabolic dispersion of the GaAs s band is strongly mixed with the flat dispersion of the AlAs p band of the AlAs bulk X point. As the width of layers decreases, the GaAs s state is confined more strongly and its energy increases and merges into the AlAs X-point energy. It is a feature of ultrathin GaAs/AlAs superlattices that these two bands appear very near each other at the bottom of the conduction band.

We can see that the conduction band too divides more or less into Fibonacci

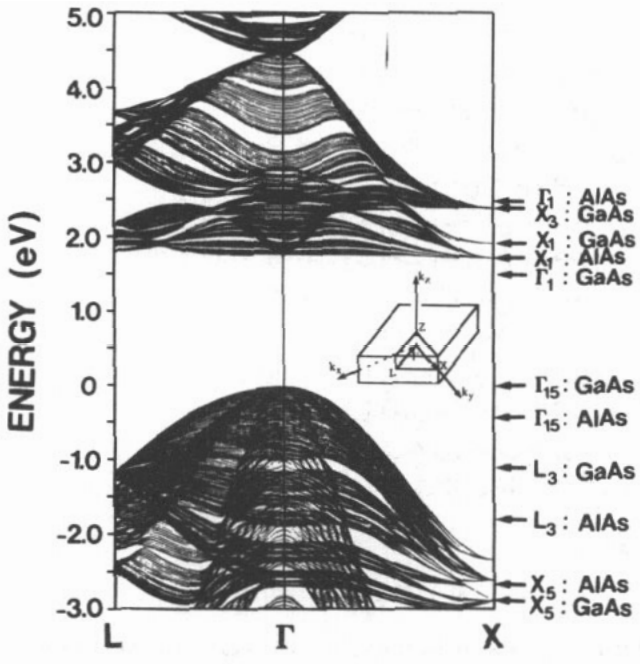

Figure 2. The band structure of the GaAs/AlAs Fibonacci superlattice for the 12th generation (144 GaAs layers and 89 AlAs layers). The positions of the energy levels in the bulk GaAs and AlAs are indicated by arrows on the right-hand side.

subbands. Above 3.0 eV this splitting is clearest, with the number of states in each subband corresponding to that expected for a Fibonacci system. At an energy between 2.5 eV and 3.0 eV, however, the dispersion around the superlattice Γ point consists of strongly hybridized GaAs s and AlAs p bands and the Fibonacci structure can no longer be observed.

The density of states at the Γ point shows the Fibonacci separation more clearly (see figure 3), than the bandstructure. As stated before, the valence band shows the self-similar energy spectrum which originates from the heavy-hole band clearly. In the conduction band, due to strong interband hybridizing, only parts of the subband structures characteristic of the Fibonacci system can be seen. In the energy region between 2.5 eV and 3.0 eV, where the s and p bands are most strongly hybridized, a spiky structure appears and the self-similar structure is destroyed. It should be noted further that for a different parallel wavevector value the energy distribution will be different due to the band dispersion parallel to the layers. Therefore the total density of states for this system will not show a Cantor-set structure.

The nature of the wavefunction is also of great interest in quasiperiodic systems, and we investigate this at the Γ point for the 12th generation GaAs/AlAs Fibonacci superlattice composed of 144 GaAs layers and 89 AlAs layers using the inverse participation ratio (IPR),

$$I_k^l = \frac{\sum |\Psi|^4}{\left(\sum |\Psi|^2\right)^2} = \frac{\sum_j^{2F_n} \sum_\alpha^5 \left|C_{j,k}^{\alpha,l}\right|^4}{\left(\sum_j^{2F_n} \sum_\alpha^5 \left|C_{j,k}^{\alpha,l}\right|^2\right)^2}. \tag{2}$$

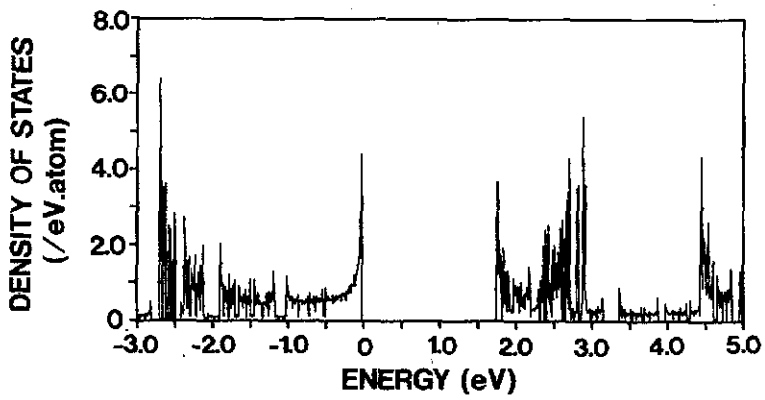

Figure 3. The density of states at the Γ point for the 12th generation GaAs/AlAs Fibonacci superlattice.

Although in general a more detailed analysis is needed to determine the exact nature of the wavefunctions, for our present purpose the IPR is sufficient. For a periodic system, the wavefunction is always extended and the IPR approaches zero as the system size increases. For a strongly localized state, the IPR is constant and large for all system sizes. In figure 4 we show the IPR versus energy level for each state at the Γ point. We see a number of steep peaks in the energy region between 2.5 eV and 3.0 eV where strong hybridization occurs and the self-similar structure is destroyed, while for the states in the other energy regions where the Fibonacci character exists in the energy spectrum, the IPR takes on an almost uniform and much smaller value.

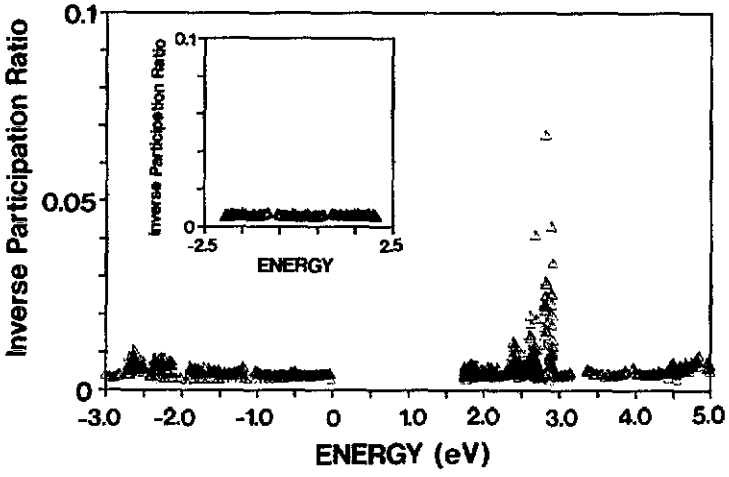

Figure 4. The IPR for the states at the Γ point for the 12th generation GaAs/AlAs Fibonacci superlattice. In the inset is the IPR for the single-band on-site model of the 12th generation with the parameters $V^A = 0.2$, $V^B = -0.2$ and $t = 1.0$.

By examining increasingly larger generations, we found in addition that the IPR for the states in the hybridized energy region varies much less with system size than the value for the other energy regions. This suggests that the localization character of the wavefunction is enhanced by the interband hybridization. We note that in the case

of a random system, the wavefunctions also show strong localization characters at the edge of the band and in the hybridized energy region, indicating that the electronic properties of the Fibonacci system are intermediate between those of the periodic superlattice and a random superlattice.

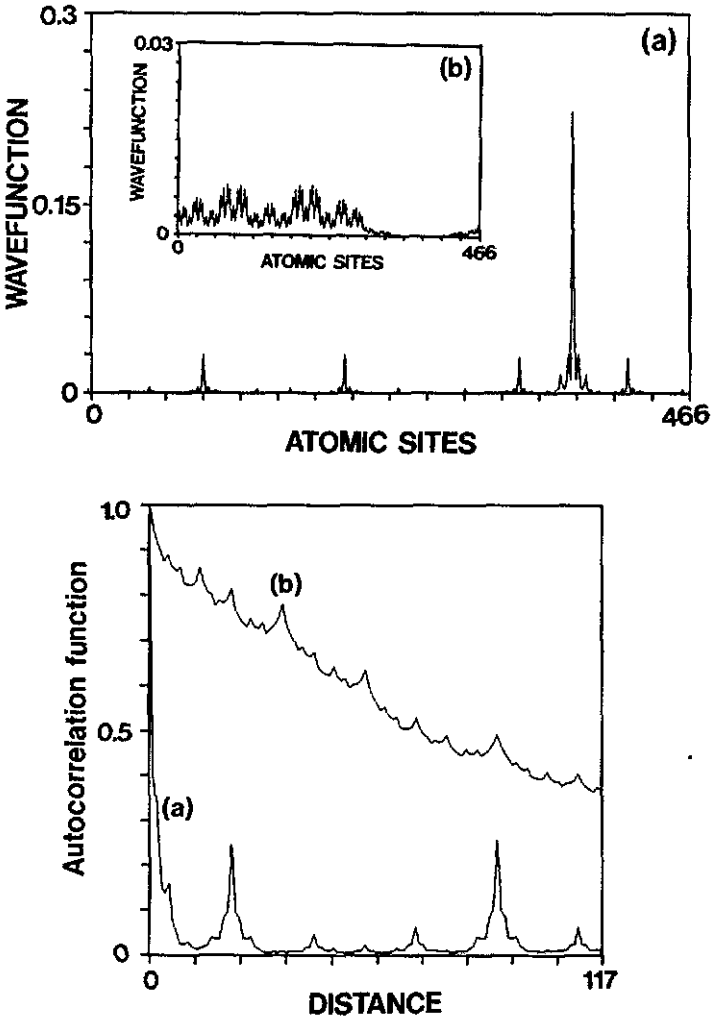

Figure 5. The wavefunction of the GaAs/AlAs Fibonacci superlattice for the 12th generation, corresponding to the state having the largest IPR (*a*). The inset is the wavefunction for the state at the bottom of the conduction band (*b*) (top). The autocorrelation function corresponding to the states (*a*) and (*b*) (bottom).

The wavefunction for the state with the largest IPR is shown in figure 5 (top). The electron amplitude is clearly concentrated in a quite narrow energy region, with weak secondary peaks existing far from it. For a comparison, the wavefunction at the bottom of the conduction band for the same Fibonacci system (at which a strong localization character would be seen for a random system) is shown in the inset. These localization characters are consistent with the IPR behaviour observed, and in order to obtain more information we examined the autocorrelation function for these

two states (see figure 5 (bottom))

$$\alpha_k^l(L) = \langle \Psi_i \Psi_{i+L} \rangle = \frac{\sum_j^{F_n} \left[\sum_\alpha^5 \left(\left| C_{2j-1,k}^{\alpha,l} \right|^2 + \left| C_{2j,k}^{\alpha,l} \right|^2 \right) \left(\sum_\alpha^5 \left| C_{2j-1+L,k}^{\alpha,l} \right|^2 + \left| C_{2j+L,k}^{\alpha,l} \right|^2 \right) \right]}{\sum_j^{F_n} \left[\sum_\alpha^5 \left(\left| C_{2j-1,k}^{\alpha,l} \right|^2 + \left| C_{2j,k}^{\alpha,l} \right|^2 \right) \right]^2} \tag{3}$$

where the As atom is located at the site number $2j-1$ and the Ga or Al atom is located at the site number $2j$. For a periodic system α is constant and for a random system α scales as $e^{-L/\xi}$ where ξ is the localization length. For a critical wavefunction the wavefunction decays by some power law. In the case of the Fibonacci superlattice, the autocorrelation function for the state with the largest IPR decreases rapidly with L, demonstrating an enhanced localization character. However this wavefunction is clearly different from that of the random system as the autocorrelation does not show exponential decay. The large correlation at the distance of the Fibonacci number is the reflection of the inherent quasiperiodic symmetry in the system and indicates that phase correlation characteristic of the Fibonacci system is not destroyed by the hybridization. Thus the wavefunction remains critical, consistent with the 1D renormalization group analysis by Chakrabarti *et al* [19].

4. The two-band model

In the previous section, we found that the localization character of a Fibonacci system may be enhanced due to interband hybridization effects. In order to clarify the situation in the hybridized energy region, we simplify the calculation by restricting ourselves to a two-band nearest-neighbour tight-binding system, with a Hamiltonian given by

$$H = \sum_i |i\rangle \begin{pmatrix} V_1^{\text{A or B}} & 0 \\ 0 & V_2^{\text{A or B}} \end{pmatrix} \langle i| + \sum_{(i,j)} |i\rangle \begin{pmatrix} t_{11} & t_{12} \\ t_{21} & t_{22} \end{pmatrix} \langle j|. \tag{4}$$

The on-site energies V^{A} and V^{B} are arranged in the Fibonacci sequence and the transfer interaction between the orbitals on the nearest neighbouring site is taken to be independent of the atomic species. Therefore this model is an extended version of the more common single-band on-site model. A schematic diagram for this model is shown in figure 6.

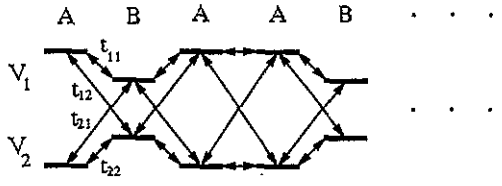

Figure 6. Schematic diagram of the two-band tight-binding model with two atomic species arranged in the Fibonacci sequence.

First we consider the transfer matrix for this two-band system, which may be expressed as

$$\begin{pmatrix} \Psi_{n+1} \\ \Psi_n \end{pmatrix} = \begin{pmatrix} X_n & -I \\ I & 0 \end{pmatrix} \begin{pmatrix} \Psi_n \\ \Psi_{n-1} \end{pmatrix} \qquad \Psi_n = \begin{pmatrix} \psi_{n,1} \\ \psi_{n,2} \end{pmatrix}. \tag{5}$$

Here

$$X_n = \frac{1}{t_{11}t_{22} - |t_{12}|^2} \begin{pmatrix} t_{22}(E - V_1) & -t_{12}(E - V_2) \\ -t_{21}(E - V_1) & t_{11}(E - V_2) \end{pmatrix} \qquad I = \begin{pmatrix} 1 & 0 \\ 0 & 1 \end{pmatrix}. \tag{6}$$

This 4×4 transfer matrix (5) has a similar form to the 2×2 transfer matrix of the single-band on-site model [8];

$$\begin{pmatrix} \psi_{n+1} \\ \psi_n \end{pmatrix} = \begin{pmatrix} (E - V_n)/t & -1 \\ 1 & 0 \end{pmatrix} \begin{pmatrix} \psi_n \\ \psi_{n-1} \end{pmatrix} \tag{7}$$

such that the denominator $t_{11}t_{22} - |t_{12}|^2$ in X_n acts as an effective hopping transfer similar to t in the 2×2 case. Thus the hopping transfer becomes almost zero when $|t_{12}|$ is close to $\sqrt{t_{11}t_{22}}$. From the band picture this situation corresponds to the creation of the flat energy dispersion and the increase of the effective mass due to the band hybridization.

In the case of the 2×2 transfer matrix, analytic approaches based on trace maps are known to be effective. For example, the trace map at the centre of the spectrum has 6 cycles [8, 10, 11] and its wavefunction has a multifractal structure [20]. As far as we know, however, trace map analysis for the present 4×4 transfer matrix is not known. Numerically, we have been unable to locate any limit cycles to an acceptable degree of accuracy. Furthermore, we have to go back to the Schrödinger equation in the case of $|t_{12}| = \sqrt{t_{11}t_{22}}$. We therefore treat this model numerically with the direct diagonalization of the Hamiltonian matrix using a rational approximation and periodic boundary condition as before.

In figure 7 we show the density of states around the two-band crossing energy region for the periodic, Fibonacci and random systems with 1597 sites (16th generation) respectively. The parameters used are $V_1^A = -V_2^A = 2.0$, $V_1^B = -V_2^B = 1.0$, $t_{11} = 1.0$, $t_{22} = 1.0$ and $t_{12} = t_{21} = 1.0$. Here $|t_{12}|$ is chosen as $|t_{12}| = \sqrt{t_{11}t_{22}}$. The density of states for the periodic system shows the existence of the gap caused by the band hybridization effect. We can see that two Van Hove singularities, characterized as $D(E) \sim 1/\sqrt{E}$, appear on both sides of the gap. For the random system, there exists a band-tail in the gap region, as expected for amorphous materials. The Fibonacci system, on the other hand, shows a spiky density of states in the gap region and other subsidary gaps open up due to the long-range quasiperiodicity. The IPR for the present Fibonacci system is shown in figure 8 (top). We see that in the hybridized energy region the IPR takes on large values indicating an enchanced localization behaviour similar to the result of the full GaAs/AlAs calculation. The dependence of the IPR on the system size is shown in figure 8 (bottom) with (1) denoting the average IPR for the states in the energy region from -5.0 to -1.0 and from 1.0 to 5.0 and (2) denoting the value for the state with the largest IPR. For reference we also show the line of $\log 1/F_n \sim -n \log \tau$, where τ is the golden mean. This line corresponds to the value expected for an extended state. We can see clearly that for case (1) the IPR falls rapidly with increasing system size, more or less according to the behaviour of an

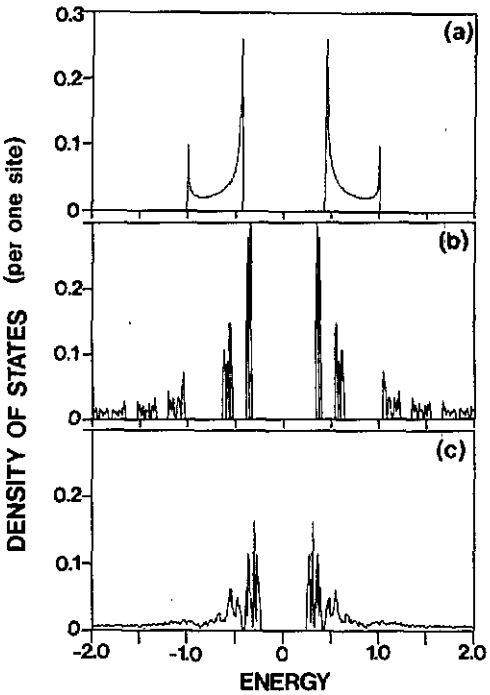

Figure 7. The density of states per site in the hybridized energy region for (*a*) a periodic system (*b*) a 16th generation Fibonacci system (1597 atoms), and (*c*) a random system. The result for (*c*) has been averaged over 30 samples.

extended state, whilst the value for case (2) is hardly changed. Our numerical results also show that the strongest localization enhancement is found where $|t_{12}| = \sqrt{t_{11}t_{22}}$, indicating that an almost zero dispersion of the hybridized state on both sides of the bandgap is essential to the development of the localization character.

One might understand this behaviour in terms of multiple scattering of a free electron with wavevector k with effective reciprocal lattice vectors $\mathbb{G}$ arising from the quasiperiodic potential [21]. As the size of the system increases, together with the almost flat energy dispersion near the edge of the bandgap such that the energy $E(k)$ and $E(k+G)$ are nearly degenerate for almost all G, the original state strongly mixes with a large number of other states, which results in the localization-like behaviour of the wavefunction. It is also said that the effective mass becomes very large and so the states are more localized. It is important to note that the appearance of large, spiky densities of states and the localization-like behaviour of the states in the gap region are due to the combined effect of the band hybridization and the long-range quasiperiodicity.

The autocorrelation function for the state with the largest IPR versus $\log_\tau L$ is shown in figure 9. We can see that large correlations appear at distances of $L = \tau^5, \tau^8, \tau^{11}, \tau^{14}$, demonstrating that the distance with large autocorrelation between the sites gets enlarged by a factor of τ^3. This character is also found for the wavefunction at the centre of the band for the single-band model. Moreover, these two wavefunctions are similar in shape. This suggests that the present wavefunction for the two-band model is not so different from that of the single-band model.

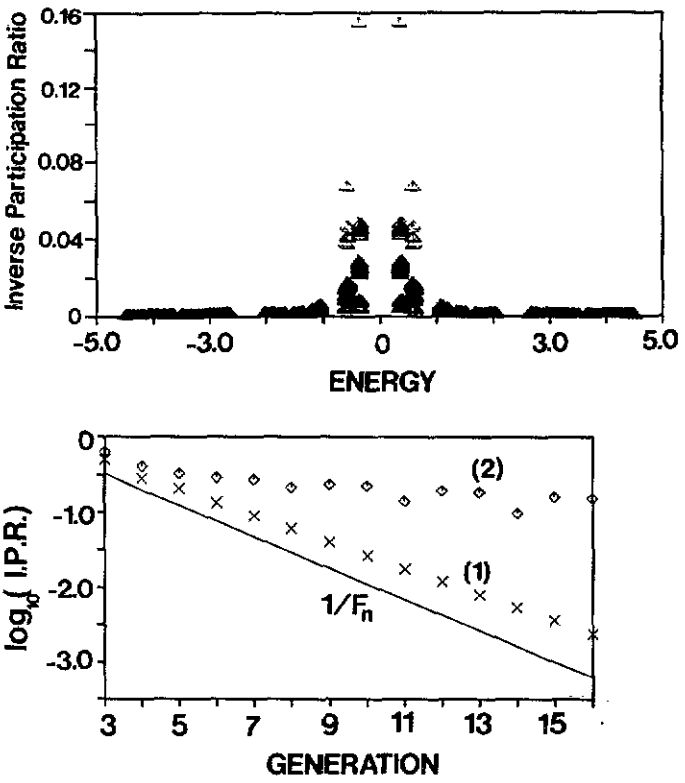

Figure 8. The inverse participation ratio for a 16th generation Fibonacci system (top). The corresponding dependences on the system size for (1) the averaged value of the IPR in the energy region from -5.0 to -1.0 and from 1.0 to 5.0 and (2) the largest IPR (bottom). The line $1/F_n$ is included as reference.

In order to obtain more information on the properties of this wavefunction, it is necessary to do the multifractal analysis and to investigate the 4×4 transfer matrix.

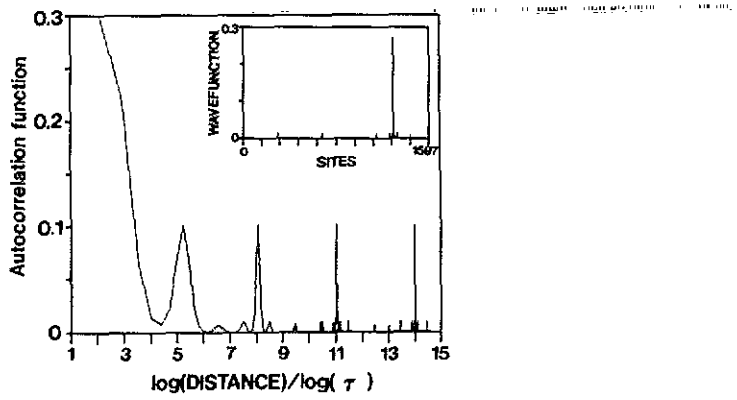

Figure 9. The autocorrelation function $\langle \Psi_i \Psi_{i+L} \rangle$ for the state with the largest IPR versus $\log_{\tau} L$. The inset shows the amplitude of the corresponding wavefunction.

5. Conclusions

In summary, we have performed a calculation of the electronic structure of the GaAs/AlAs Fibonacci superlattice with the sp^3s^* model with use of a semi-empirical tight-binding method. We have found that, although the energy spectrum is strongly dependent on the wavevector perpendicular to the superlattice direction, a self-similar energy spectrum can be seen both in the valence band and in the conduction band for a given parallel wavevector. The X point is special in that the Fibonacci structure collapses there. We have also found that the band hybridization between the s band of GaAs and the p band of AlAs around the Γ point in the conduction band destroys the appearance of a self-similar energy spectrum at the energy level between 2.5 eV and 3.0 eV. The wavefunctions corresponding to these states reveal an enhanced localization behaviour, even though the wavefunction remains critical. Such localization-like behaviour is also seen in the hybridized energy region in a two-band tight-binding model and may be due to the strong multiple scattering of electrons as a result of the existence of nearly degenerate states and a long-range quasiperiodicity. The analysis of the wavefunction with the largest IPR shows that the distance of large autocorrelation between the sites gets enlarged by a factor of τ^3. This suggests that the phase correlation characteristic of the Fibonacci system remains and this wavefunction is related to the band centre state in the single-band model.

Acknowledgments

We are indebted to Professors M Tsukada, H Aoki, and to Drs T Nakayama, T Hatakeyama, and A A Yamaguchi for valuable discussions. We would like to thank Dr E Yamaguchi of the NTT Basic Reseach Laboratory for the sp^3s^* model calculation. This work was partly supported by Grant-in-Aid from the Ministry of Education, Science and Culture of Japan. One of us (DYKK) is grateful for financial support from the Japan Society for the Promotion of Science, and KH acknowledges the Department of Theoretical Physics, University of Oxford where part of the work was carried out. The numerical calculations were performed by the HITAC S-820 computer system at the computer centre of the University of Tokyo.

References

[1] Shechtman D, Blech I, Gratias D and Cahn J W 1984 *Phys. Rev. Lett.* **53** 1951
[2] Levine D and Steinhardt P J 1984 *Phys. Rev. Lett.* **53** 2477
[3] Niu Q and Nori F 1986 *Phys. Rev. Lett.* **57** 2057
[4] Niu Q and Nori F 1990 *Phys. Rev.* B **42** 10329
[5] Liu Y and Riklund R 1987 *Phys. Rev.* B **35** 6034
[6] Fujita M and Machida K 1986 *Solid State Commun.* **59** 61
[7] Ninomiya T 1986 *J. Phys. Soc. Japan* **55** 3709
[8] Kohmoto M, Kadanoff L P and Tang C 1983 *Phys. Rev. Lett.* **50** 1870
[9] Ostlund S, Pandit R, Rand D, Schellnhuber H J and Siggia E D 1983 *Phys. Rev. Lett.* **50** 1873
[10] Kohmoto M and Benavar J R 1986 *Phys. Rev.* B **34** 563
[11] Kohmoto M, Sutherland B and Tang C 1987 *Phys. Rev.* B **35** 1020
[12] Merlin R, Bajema K, Juang F Y and Bhattacharya P K 1985 *Phys. Rev. Lett.* **55** 1768
[13] Todd J, Merlin R, Clarke R, Mohanty K M and Axe J D 1986 *Phys. Rev. Lett.* **57** 1157
[14] Yamaguchi A A, Saiki T, Tada T, Ninomiya T, Misawa K, Kobayashi T, Gonokami M K and Yao T 1990 *Solid State Commun.* **75** 955

[15] Vogl P, Hjalmarson H P and Dow J D 1983 *J. Phys. Chem. Solids.* **44** 365
[16] Newman K E and Dow J D 1984 *Phys. Rev.* B **30** 1929
[17] Yamaguchi E 1987 *J. Phys. Soc. Japan* **56** 2835
[18] Yamaguchi E 1986 *Japan. J. Appl. Phys.* **25** L643
[19] Chakrabarti A, Karmakar S N and Moitra R K 1990 *Mod. Phys. Lett.* B **4** 795
[20] Fujiwara T, Kohmoto M and Tokihiro T 1989 *Phys. Rev.* B **40** 7413
[21] Smith A P and Ashcroft N W 1987 *Phys. Rev. Lett.* **59** 1365